Int. J. Engng Sci. Vol. 31 No. 9, pp. 1309–1323, 1993
Printed in Great Britain.
0020-7225/93 $6.00 + 0.00

STEADY STATE AXISYMMETRIC PENETRATION OF A KINEMATICALLY HARDENING THERMOVISCOPLASTIC TARGET

R. C. BATRA
Department of Mechanical and Aerospace Engineering and Engineering Mechanics, University of Missouri–Rolla, Rolla, MO 65401-0249, U.S.A.

R. JAYACHANDRAN
Department of Mechanical Engineering, Massachusetts Institute of Technology, Cambridge, MA 02139, U.S.A.

Abstract—We study axisymmetric thermomechanical deformations of a thick target being penetrated by a fast-moving rigid cylindrical rod with a hemispherical nose, and presume that target deformations appear steady to an observer situated at the penetrator nose tip. Both isotropic and kinematic hardening of the target material are considered. It is found that kinematic hardening increases the normal stress acting on the penetrator nose surface and the temperature rise of target particles abutting the penetrator. However, the value of the hydrostatic pressure at a point in the deforming target region is affected very little by the consideration of kinematic hardening. For suitable values of material parameters appearing in the evolution equation of the back-stress, the computed values of the back-stress at target particles abutting the penetrator nose surface equal three times the yield stress of the target material in a quasistatic simple compression test.

1. INTRODUCTION

During the penetration of a thick target by a fast-moving cylindrical rod, target and penetrator material particles in the vicinity of the target/penetrator interface are deformed severely, and are also heated up significantly. Consequently, the material undergoes microstructural changes such as the generation/annihilation of dislocations, dynamic recovery and recrystallization, development of texture, nucleation and growth of microcracks and voids, and possibly the development of shear bands that form during the intense plastic deformations of a material, especially at high strain rates. One way to account for these microstructural changes is to use constitutive equations which employ a suitable number of scalar and tensor valued internal variables (e.g. see Coleman and Gurtin [1], Chan *et al.* [2], Inoue [3], Lubliner [4], and Anand [5]). Here we use one scalar variable to describe the isotropic hardening, and a traceless symmetric second-order tensor, also known as the back stress tensor, to account for the kinematic hardening of the material. The Litonski–Batra constitutive relation (e.g. see Batra and Jayachandran [6]) is modified to incorporate the kinematic hardening and used herein to study the thermomechanical axisymmetric deformations of the target. The hemispherical nosed cylindrical penetrator is assumed to be rigid and the target deformations steady, as seen by an observer situated at the penetrator nose tip and moving with it. We note that Batra and Jayachandran [6] recently analyzed thermomechanical deformations of a target by using three constitutive relations, namely, those due to Litonski–Batra, Bodner–Partom [7], and Brown *et al.* [8]. Each of these was calibrated to give almost identical effective stress vs logarithmic strain curves for a block made of target material and deformed in plane strain compression at an average strain-rate of $3300\,s^{-1}$. Even though these constitutive relations account for the evolution of the microstructural changes in different ways, they gave essentially identical results for the resisting force experienced by the penetrator, normal stress on the penetrator nose surface, and the distribution of the tangential speed and the second-invariant of the strain-rate tensor on the penetrator nose surface.

This work is in the spirit of the one initiated by Batra and Wright [9], and is aimed at providing guidelines for selecting and improving upon the previously used kinematically admissible fields in engineering models of target penetration. Subsequently, Batra and co-workers [10–19] have studied different aspects of the problem. Review articles by Backman and Goldsmith [20], Wright and Frank [21], and Anderson and Bodner [22], and books by Blazynski [23], MaCauley [24], and Zukas *et al.* [25, 26] provide a summary of the work completed on the penetration problem. For penetration speeds in the range of 0.5–10 km/s, Birkhoff *et al.* [27], Pack and Evan [28], Allen and Rogers [29], Alekseevskii [30], and Tate [31] have proposed using the Bernoulli equation or its modification to study the steady state penetration process. The last three references introduced a resistive pressure, dependent upon the material strength, in the Bernoulli equation. Tate [32–34] used a solenoid fluid flow model of the steady state penetration process to estimate the resistive pressure, and Batra *et al.* [10–12] and Pidsley [35] used a numerical solution of the governing equations to find the resistive pressure. Engineering models of different complexity have been proposed by Awerbuch [36], Awerbuch and Bodner [37], Ravid and Bodner [38], Ravid *et al.* [39], Forrestral *et al.* [40], and Batra and Chen [41]. Chen and Batra [42] proposed an expression for the frictional force on the target/penetrator interface in terms of the relative speed of sliding of target particles on the penetrator nose surface and the normal traction acting there.

2. FORMULATION OF THE PROBLEM

With respect to a cylindrical coordinate system with origin attached to the center of the hemispherical penetrator nose and positive z-axis pointing into the target, equations governing the axisymmetric steady deformations of the target are:

Balance of mass

$$\operatorname{div} \mathbf{v} = 0, \tag{1}$$

Balance of linear momentum

$$\operatorname{div} \boldsymbol{\sigma} = \rho(\mathbf{v} \cdot \operatorname{grad})\mathbf{v}, \tag{2}$$

Balance of internal energy

$$-\operatorname{div} \mathbf{q} + \operatorname{tr}(\boldsymbol{\sigma}\mathbf{D}^{\mathrm{p}}) = \rho(\mathbf{v} \cdot \operatorname{grad})U, \tag{3}$$

where

$$2\mathbf{D} = \operatorname{grad} \mathbf{v} + (\operatorname{grad} \mathbf{v})^{\mathrm{T}}, \qquad 2\mathbf{W} = \operatorname{grad} \mathbf{v} - (\operatorname{grad} \mathbf{v})^{\mathrm{T}}, \tag{4}$$

$$\mathbf{q} = -k \operatorname{grad} \theta, \tag{5}$$

$$U = c\theta, \tag{6}$$

$$\boldsymbol{\sigma} = -p\mathbf{1} + \mathbf{s}, \tag{7}$$

$$\dot{\mathbf{s}} \equiv (\mathbf{v} \cdot \operatorname{grad})\mathbf{s} + \mathbf{sW} - \mathbf{Ws} = 2G(\mathbf{D} - \mathbf{D}^{\mathrm{p}}), \tag{8}$$

$$\mathbf{s} - \mathbf{B} = 2\mu(I, \theta, \psi)\mathbf{D}^{\mathrm{p}}, \tag{9}$$

$$\dot{\mathbf{B}} = (\mathbf{v} \cdot \operatorname{grad})\mathbf{B} + \mathbf{BW} - \mathbf{WB} = \xi_1\mathbf{D}^{\mathrm{p}} - \xi_2 I\mathbf{B}, \qquad \operatorname{tr} \mathbf{B} = 0, \tag{10}$$

$$2\mu(I, \theta, \psi) = \frac{\sigma_0}{\sqrt{3}\,I}(1 + bI)^m(1 - \nu\theta)\left(1 + \frac{\psi}{\psi_0}\right)^n, \tag{11}$$

$$\dot{\psi} \equiv (\mathbf{v} \cdot \operatorname{grad})\psi = \frac{\operatorname{tr}(\boldsymbol{\sigma}\mathbf{D}^{\mathrm{p}})}{\sigma_0\left(1 + \dfrac{\psi}{\psi_0}\right)^n}, \tag{12}$$

$$2I^2 = \operatorname{tr}(\mathbf{D}^{\mathrm{p}})^2. \tag{13}$$

Here $\mathbf{v}$ is the velocity of a material particle, $\boldsymbol{\sigma}$ the Cauchy stress tensor at the present location of a material particle, ρ the mass density, $\mathbf{q}$ the heat flux, $\mathbf{D}$ the stretching tensor, and $\mathbf{W}$ the spin tensor. The balance laws (1), (2), and (3) are written in the Eulerian description of motion, and the operators grad and div denote the gradient and divergence operators on fields defined in the present configuration. Equation (1) implies that both the elastic and plastic deformations of the target are assumed to be isochoric. Equation (5) is the Fourier law of heat conduction with k the thermal conductivity and θ the temperature rise of a material particle. Equation (6) is the presumed constitutive relation for the specific internal energy U, wherein c is the specific heat. In equations (7)–(13), $\boldsymbol{\sigma}$ is the Cauchy stress tensor, $\mathbf{s}$ its deviatoric part, p the hydrostatic pressure not determined by the deformation history, $\mathbf{B}$ the traceless symmetric second-order tensor used to account for the kinematic hardening of the material, and ψ is a scalar internal variable that accounts for the isotropic hardening of the material. The evolution equation (10) for $\mathbf{B}$ has been proposed by White *et al.* [43]. Equation (9) with μ given by equation (11) is a generalization of the Litonski–Batra law to account for the kinematic hardening of the material. Here σ_0 is the yield stress in a quasistatic simple tension or compression test, parameters b and m characterize the strain-rate sensitivity of the material, v its thermal softening, and b its workhardening. In a quasistatic simple tension or compression test,

$$\sigma = \sigma_0\left(1 + \frac{\psi}{\psi_0}\right)^n$$

describes the stress–strain curve, where ψ is now interpreted as the plastic strain. In a dynamic test, the effect of the history of deformation upon the present state of deformation is accounted for through the parameter ψ.

We nondimensionalize variables by scaling stress-like quantities by σ_0, length by r_0, time by (r_0/v_0), and the temperature by the reference temperature θ_r, defined by

$$\theta_r \equiv \sigma_0/\rho c. \tag{14}$$

Here r_0 equals the radius of the cylindrical part of the penetrator and v_0 the penetration speed. In terms of nondimensional variables, the aforestated governing equations become

$$\operatorname{div} \mathbf{v} = 0, \tag{15.1}$$

$$-\operatorname{grad} p + \operatorname{div} \mathbf{s} = \alpha(\mathbf{v} \cdot \operatorname{grad})\mathbf{v}, \tag{15.2}$$

$$\mathbf{s} - \mathbf{B} + \beta\gamma((\mathbf{v} \cdot \operatorname{grad})\mathbf{s} + \mathbf{sW} - \mathbf{Ws}) = 2\beta\mathbf{D}, \tag{15.3}$$

$$\operatorname{tr}(\boldsymbol{\sigma}\mathbf{D}^p) + \delta \operatorname{div}(\operatorname{grad} \theta) = (\mathbf{v} \cdot \operatorname{grad})\theta, \tag{15.4}$$

$$(\mathbf{v} \cdot \operatorname{grad})\mathbf{B} + \mathbf{BW} - \mathbf{WB} + \xi_2 I\mathbf{B} = \xi_1\mathbf{D}^p, \tag{15.5}$$

$$(\mathbf{v} \cdot \operatorname{grad})\psi = \operatorname{tr}(\boldsymbol{\sigma}\mathbf{D}^p)\Big/\left(1 + \frac{\psi}{\psi_0}\right)^n, \tag{15.6}$$

where

$$\alpha = \frac{\rho v_0^2}{\sigma_0}, \quad \beta = \frac{\mu v_0}{\sigma_0 r_0}, \quad \gamma = \frac{\sigma_0}{G}, \quad \text{and} \quad \delta = \frac{k}{\rho c v_0 r_0} \tag{15.7}$$

are nondimensional numbers. Henceforth, we will use nondimensional variables only. For a given problem, α, γ, and δ are constants, but β varies from point to point in the deforming region because of the variation in μ. The value of α signifies the importance of inertia forces relative to the flow stress of the material, and may be thought of as the reciprocal of the Reynolds number in a viscous fluid. The values of γ and δ give the effect of material elasticity and heat conduction, respectively. For typical penetration problems involving long rod penetrators, δ is of the order of 10^{-5}; hence target deformations may be considered adiabatic.

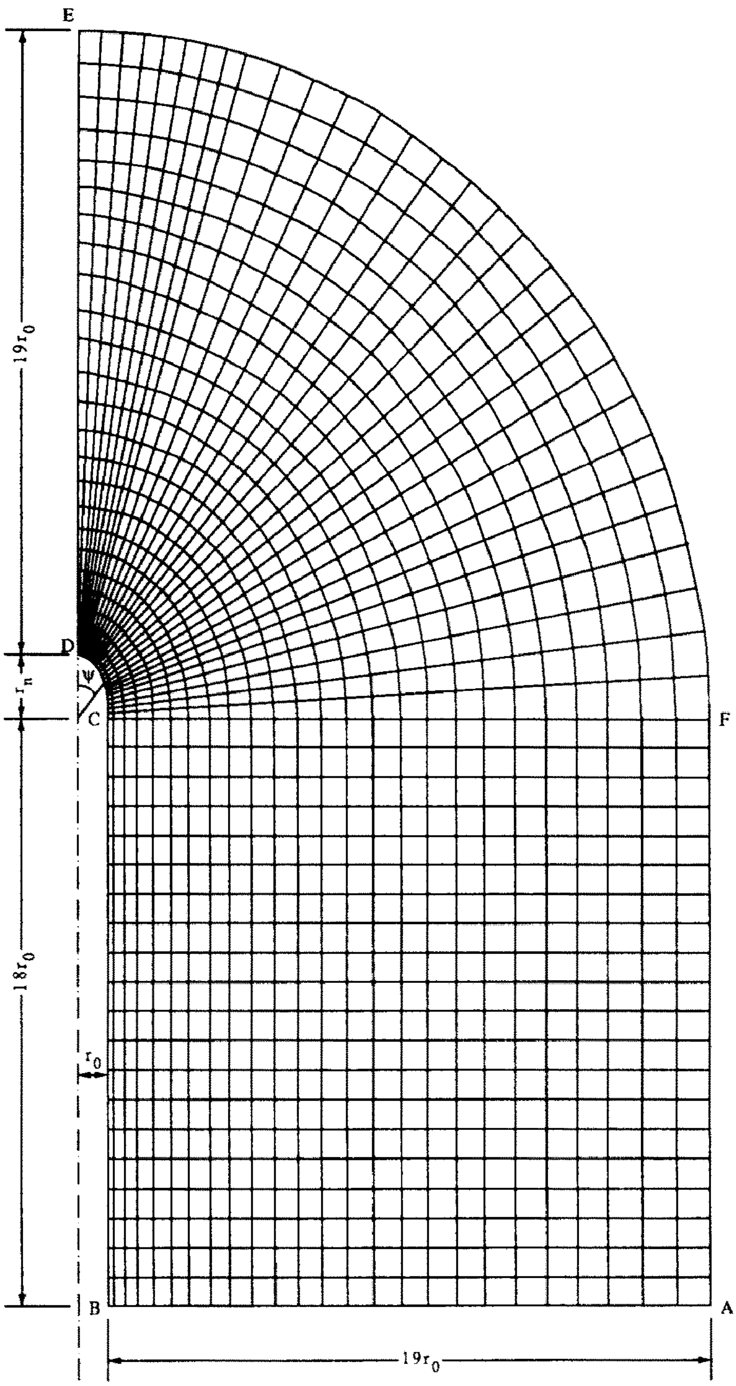

Fig. 1. The finite region studied and its finite element discretization.

Before stating boundary conditions, we note that the governing equations (15) are highly nonlinear and coupled, and are very difficult, if not impossible, to analyze. Here we seek their approximate solution by the finite element method, which necessitates that we consider a finite region of the target. The finite target region studied is shown in Fig. 1, and we impose on it the following boundary conditions.

$$\mathbf{t}\cdot(\boldsymbol{\sigma}\mathbf{n}) = 0 \qquad \text{on } \Gamma_i, \tag{16.1}$$

$$\mathbf{v}\cdot\mathbf{n} = 0 \qquad \text{on } \Gamma_i, \tag{16.2}$$

$$\mathbf{q}\cdot\mathbf{n} = h_c(\theta - \theta_a) \qquad \text{on } \Gamma_i, \tag{16.3}$$

$$\sigma_{zz} = 0, \qquad v_r = 0, \qquad \frac{\partial \theta}{\partial z} = 0 \quad \text{on the surface AB,} \tag{16.4}$$

$$v_r = 0, \quad v_z = -1, \quad \theta = 0, \quad \psi = 0, \quad p = 0, \quad s_{rr} = 0, \quad s_{\theta\theta} = 0, \quad s_{zz} = 0,$$
$$s_{rz} = 0, \quad B_{rr} = 0, \quad B_{\theta\theta} = 0, \quad B_{zz} = 0, \quad B_{rz} = 0 \quad \text{on the bounding surface EFA,} \tag{16.5}$$

$$\sigma_{rz} = 0, \qquad v_r = 0, \qquad \frac{\partial \theta}{\partial r} = 0 \quad \text{on the axis of symmetry DE.} \tag{16.6}$$

Here **n** and **t** denote, respectively, a unit normal and a unit tangent vector to the surface, θ_a is an average temperature of the penetrator, h_c is the heat transfer coefficient between the penetrator and the target, and Γ_i denotes the target/penetrator interface. The boundary conditions (16) incorporate the assumptions that Γ_i is smooth, there is no interpenetration of the target material into the penetrator and vice versa, the deformations are axisymmetric, and the bounding surfaces AB and EFA are far removed from the penetrator nose surface. The boundary conditions (16.5) on p and components of **s** and **B** on the surface EFA are needed, since we solve equations (15.3) and (15.5) for **s** and **B**, along with the other equations for p, **v**, θ, and ψ; e.g. see Shimazaki and Thompson [44].

We refer the reader to [10] for details of obtaining a finite element solution of the problem, and ensuring that the region R studied herein is adequate. The computer code used to analyze the thermomechanical problem discussed in [6] was modified to include the effect of kinematic hardening.

3. NUMERICAL RESULTS

In an attempt to study the effect of kinematic hardening on the solution variables, the values of material parameters ξ_1 and ξ_2 in equation (15.5) were varied over a wide range. However, the other material and geometric parameters were assigned the following values, taken from [6], for an HY-100 steel.

$$\begin{gathered}
\rho = 7860\,\text{kg/m}^3, \quad \sigma_0 = 405\,\text{MPa}, \quad G = 80\,\text{GPa}, \quad c = 473\,\text{J/kg°C}, \\
k = 50\,\text{W/m°C}, \quad h = 20\,\text{W/m}^{2\circ}\text{C}, \quad \theta_a = 0, \quad r_0 = 10\,\text{mm}, \quad b = 10\,\text{s}, \\
v = 1.2 \times 10^{-3}/\text{°C}, \quad \psi_0 = 0.1, \quad m = 0.01, \quad n = 0.13, \quad \alpha = 2.0.
\end{gathered} \tag{17}$$

Thus, the reference temperature used to nondimensionalize the temperature rise equals 108.9°C.

Wang and Batra [45] have recently studied the initiation and growth of shear bands in a thermally softening viscoplasitc block obeying constitutive relations similar to equations (8)–(12) and deformed in plane strain compression at an average strain-rate of $5000\,\text{s}^{-1}$. Their load-displacement curves (cf. Fig. 10 of [45]) for the homogeneous block show that an increase in the value of ξ_1 hardens the material and an increase in the value of ξ_2 softens it in the sense that the load required to compress the block by a certain amount is more for higher values of ξ_1 and less for larger values of ξ_2. Earlier computations by Batra and Jayachandran [6] and Jayachandran and Batra [19] suggest that a change in the values of ξ_1 and ξ_2 should affect the deformations of the target in an analogous manner.

All of the results presented below and values of variables indicated in figures, unless stated otherwise, are nondimensional.

3.1 *Results with ξ_2 varied*

Figure 2 depicts the distribution of the normal stress, temperature rise, tangential speed, and the second invariant of the strain-rate tensor, also referred to as the strain-rate measure, on the

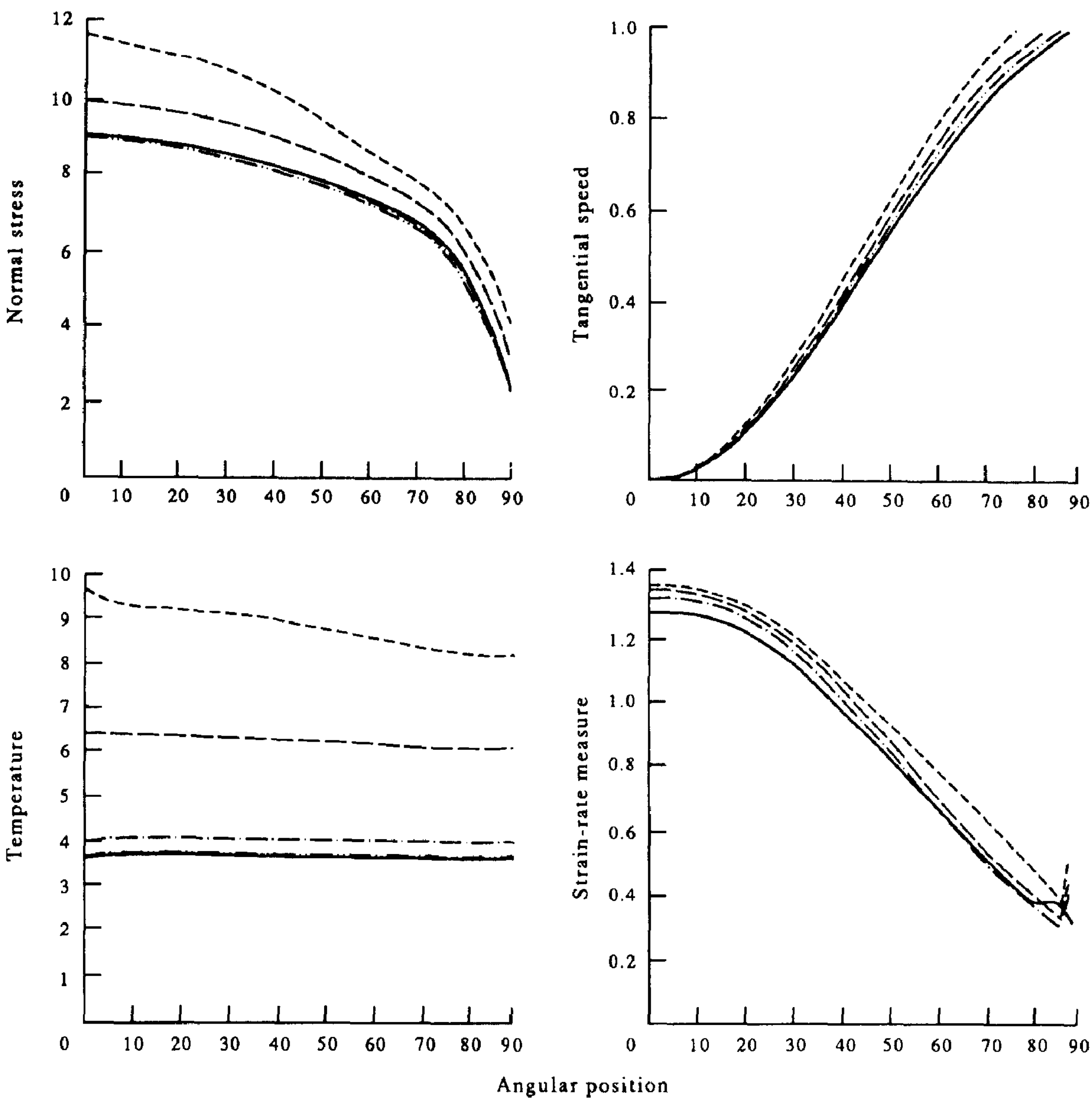

Fig. 2. Distribution of the normal stress, tangential speed, temperature rise, and the second invariant of the strain-rate tensor on the hemispherical nose surface of the penetrator for $\xi_1 = 1.0$ and four different values of ξ_2. —— no kinematic hardening; - - - $\xi_2 = 0.0$; ----- $\xi_2 = 1.0$; - · - $\xi_2 = 10.0$; - · · · - $\xi_2 = 100.0$.

penetrator nose surface for $\xi_1 = 1.0$ and $\xi_2 = 0$, 1.0, 10.0, and 100.0. We have also included the result, taken from [6], when there is no back-stress, i.e. $\xi_1 = \xi_2 = 0$. The angular position ψ, indicated in Fig. 1, is measured from the centroidal axis. For a fixed value of ξ_1, an increase in the value of ξ_2 increases the recovery term in the expression (10) for the evolution of the back-stress. The computed results indicate that the normal stress on the penetrator nose surface is essentially the same for $\xi_2 = 10$ and 100. However, lower values of ξ_2 influence significantly the distribution of the normal stress, temperature rise, tangential speed, and the strain rate measure on the penetrator nose surface. The observation that the hydrostatic pressure p at the stagnation point equals 8.71, 8.53, 8.37, and 8.34 for $\xi_2 = 0$, 1, 10, and 100, respectively, suggests that changes in the value of the normal stress are due to higher values of the deviatoric stresses which are necessitated by the evolution of the back stress there since the plastic deformation depends upon $(\mathbf{s} - \mathbf{B})$. The nondimensional axial resisting force F experienced by the penetrator and given by

$$F = \int_0^{\pi/2} (\mathbf{n} \cdot \sigma\mathbf{n}) \sin 2\phi \, d\phi \tag{18}$$

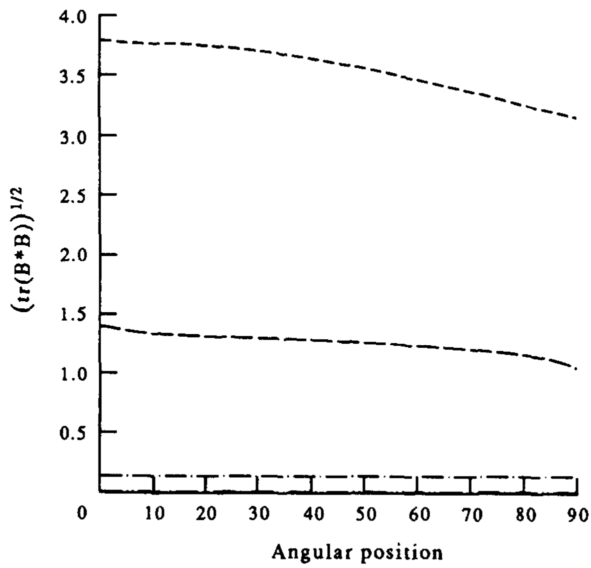

Fig. 3. Distribution of $(\mathrm{tr}\,(\mathbf{B}\,\mathbf{B}^{\mathrm{T}}))^{1/2}$ upon the penetrator nose surface for $\xi_1 = 1.0$ and four different values of ξ_2. See Fig. 2 for the legend to curves. The curve for $\xi_2 = 100$ essentially coincides with the horizontal axis.

for the hemispherical nose surface was found to equal 7.87 for the case of no kinematic hardening, and 9.61, 8.57, 7.86, and 7.77 for $\xi_2 = 0$, 1, 10, and 100, respectively. The dimensional values of F are obtained by multiplying the nondimensional ones by $\pi r_0^2 \sigma_0$. Note that in our work the speed of penetration is kept fixed, and whatever additional energy is required for the penetration process is presumed to be available. The noticeable increase in the temperature rise for $\xi_2 = 0$, 1, and 10 is due to the significant values of $\mathbf{B}$, see Fig. 3, and the observation, verified by the computed results that $\mathrm{tr}(\mathbf{BD}^{\mathrm{p}}) \geq 0$. Since values of $(\mathbf{s} - \mathbf{B})$ affect the plastic deformations of the material, an increase in the value of $\mathbf{B}$ will necessitate higher values of $\mathbf{s}$, which will cause more plastic working and, hence, greater temperature rise. The variation of the strain-rate measure, axial stress, temperature rise, and the axial velocity on the central line plotted in Fig. 4 reveals that the consideration of kinematic hardening affects these variables at points situated at most one penetrator radius from the penetrator nose tip.

An integration of equation (15.2) along the central streamline ($r = 0$) gives

$$\frac{1}{2}\alpha v^2 + p - s_{zz} - 2\int_0^z \frac{\partial \sigma_{rr}}{\partial r}\,\mathrm{d}z = -\sigma_{zz}(0). \tag{19}$$

Setting $z = 0$ and comparing the result with Tate's equation [33, 34], we get

$$R_t = -\sigma_{zz}^{s} - \frac{\alpha}{2} \tag{20}$$

where R_t equals the strength parameter for the target in Tate's equation, and σ_{zz}^{s} is the value of σ_{zz} at the stagnation point. The computed values of R_t for $\xi_2 = 0$, 1, 10, and 100 were found to be 10.63, 8.91, 8.05, and 7.97, respectively. For the case of no kinematic hardening, $R_t = 8.01$. According to Tate [33, 34],

$$R_t = \frac{2}{3} + \ln\left(\frac{2}{3}\frac{E}{\sigma_0}\right) \tag{21}$$

where E equals Young's modulus for the target material. Thus, Tate's formula gives $R_t = 6.64$. We note that for $\xi_2 = 0$ and 1, the values of s_{zz}^{s} were higher than those for $\xi_2 = 10$ and 100. Since the plastic deformation is governed by $(s_{zz} - B_{zz})$, higher values of B_{zz} necessitate a corresponding increase in the values of s_{zz}. For $\xi_2 = 0$, 1, 10, and 100, the values of $-s_{zz}(0)$

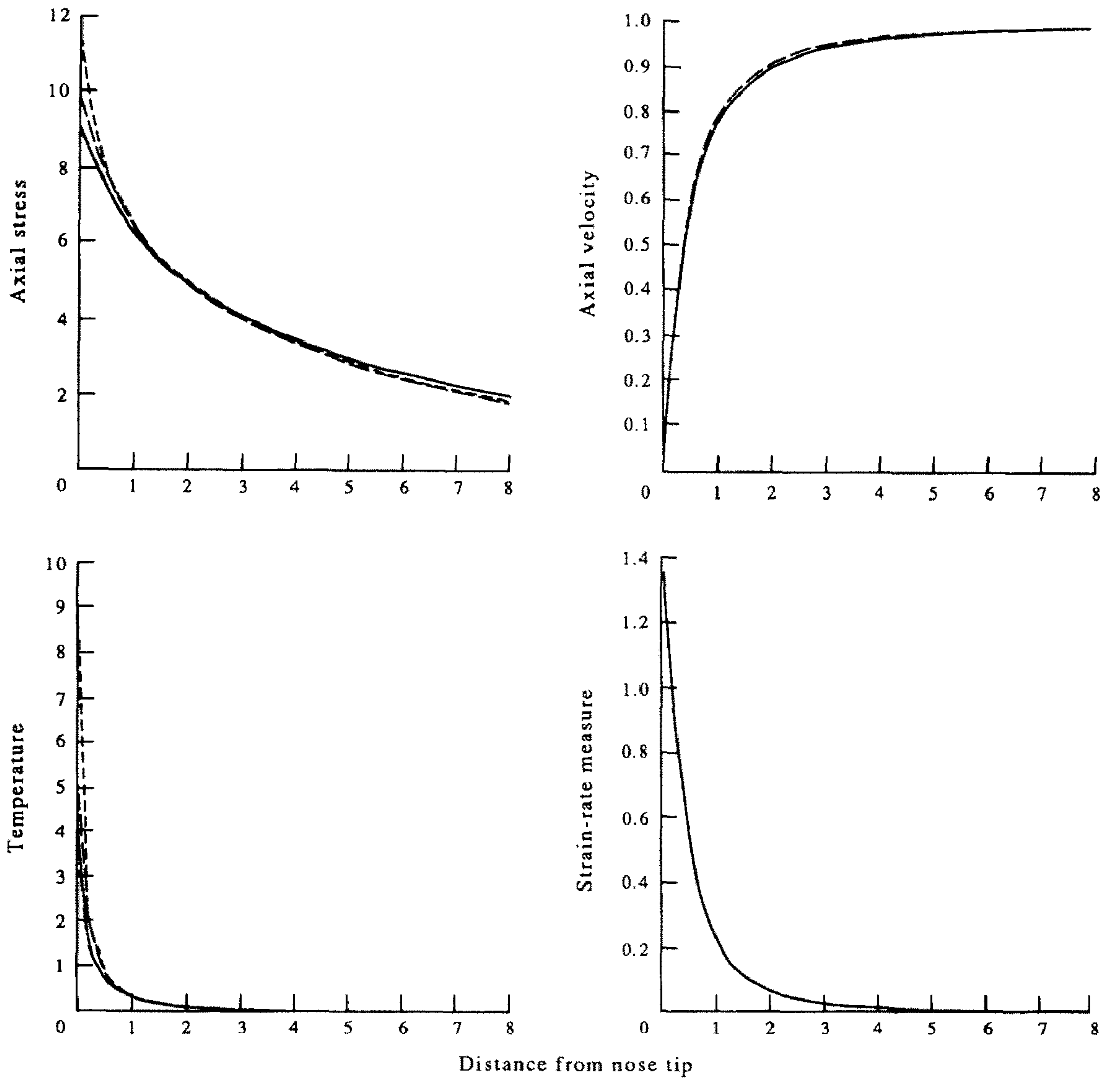

Fig. 4. Distribution of the axial stress, axial speed, temperature rise, and second invariant of the strain-rate tensor on the axial line for $\xi_1 = 1.0$ and four different values of ξ_2. See Fig. 2 for the legend to curves.

were found to be 2.92, 1.38, 0.68, and 0.63, respectively. However, the hydrostatic pressure equaled 8.71, 8.53, 8.37, and 8.34 for $\xi_2 = 0$, 1, 10, and 100.

In order to delineate whether or not the aforestated dependence of solution variables upon ξ_2 is typical, we have plotted in Fig. 5 results for $\xi_1 = 10^4$, and $\xi_2 = 10^8$, 10^6, 10^5, 6.5×10^4. Even though ξ_2 varies by three orders of magnitude, the change in the normal stress and the tangential speed on the penetrator nose surface is minimal. Furthermore, the increase in the temperature rise is considerably less than that for results plotted in Fig. 2, wherein ξ_2 was also varied by three orders of magnitude. These results suggest that the best values of ξ_1 and ξ_2 affect significantly the changes in the solution variables caused by the same relative change in the value of ξ_2. The axial resisting force experienced by the penetrator was virtually unaffected by the change in the value of ξ_2, and essentially equaled that for the case of no kinematic hardening. The distribution of $(\mathrm{tr}(\mathbf{B}^2))^{1/2}$ on the penetrator nose surface shown in Fig. 6 reveals that the values of $\mathbf{B}$ for these values of ξ_1 and ξ_2 are much lower than those for the previous case for which results are given in Fig. 3. The values of the target resistance parameter R_t were determined to be 7.96, 7.98, 7.78, and 7.70 for $\xi_2 = 10^8$, 10^6, 10^5, and 6.5×10^4, respectively.

Along the axial line, uniaxial strain conditions prevail approximately. Thus, the magnitude of

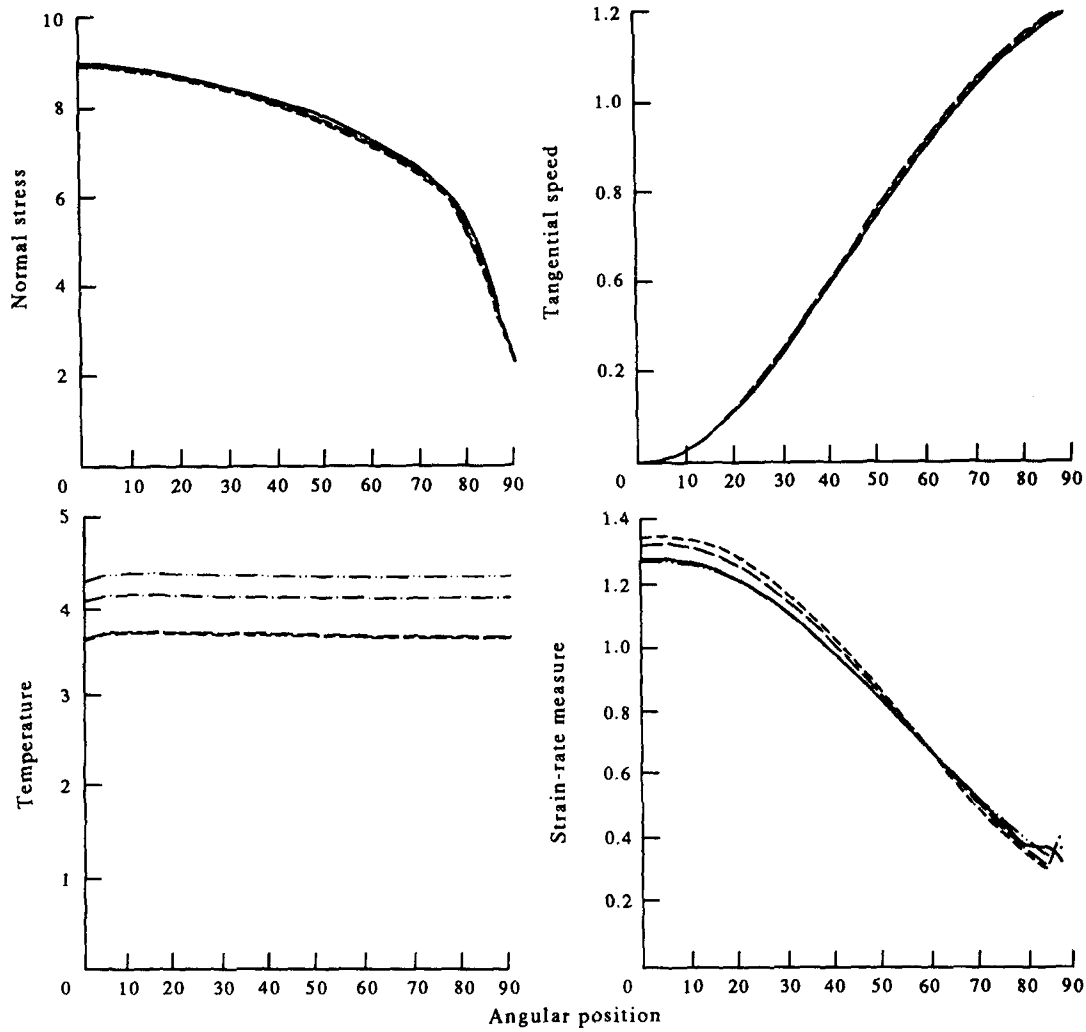

Fig. 5. Distribution of the normal stress, tangential speed, temperature rise, and the second invariant of the strain-rate tensor on the hemispherical nose surface of the penetrator for $\xi_1 = 10^4$ and four different values of ξ_2. —— no kinematic hardening; - - - $\xi_2 = 10^8$; ----- $\xi_2 = 10^6$; — · — $\xi_2 = 10^5$; — · · — $\xi_2 = 6.5 \times 10^4$.

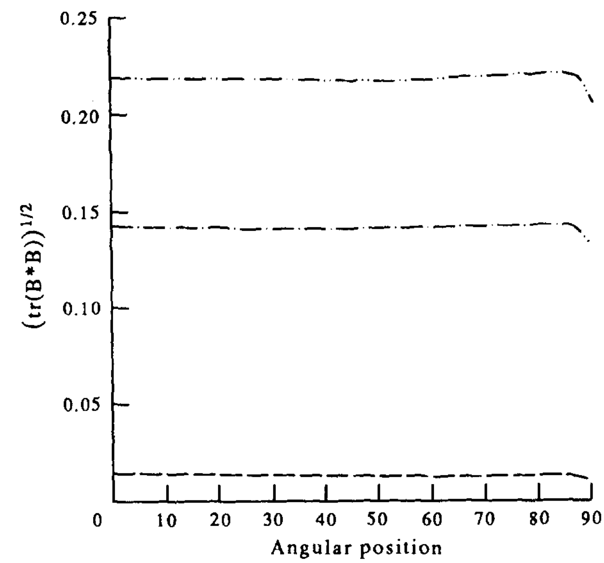

Fig. 6. Distribution of $(\mathrm{tr}(\mathbf{B}\,\mathbf{B}^T))^{1/2}$ upon the penetrator nose surface for $\xi_1 = 10^4$ and four different values of ξ_2. See Fig. 5 for the legend to curves. The curve for $\xi_2 = 10^8$ coincides with the horizontal axis.

$(s_{zz} - B_{zz})$ at a point on the axial line should equal 2/3 the effective flow stress defined as

$$\sigma_{\text{eff}} = 2\sqrt{3}\,\mu I. \tag{22}$$

For $\xi_1 = \xi_2 = 100$, the computed values of the error $e(z)$ given by

$$e(z) = 100\frac{\left|\frac{2}{3}\sigma_{\text{eff}} - |(s_{zz} - B_{zz})|\right|}{\frac{2}{3}\sigma_{\text{eff}}} \tag{23}$$

were found to be less than 2 for $1 \leq z \leq 7$ with the highest value of 1.94 occurring at $z = 1$ and 7. Thus, $|s_{zz} - B_{zz}| = \frac{2}{3}\sigma_{\text{eff}}$ holds well on the axial line.

3.2 Results with ξ_1 varied

With $\xi_2 = 100.0$ and ξ_1 assigned values 0.1, 1.0, 10, and 100, computed values of the normal stress, temperature rise, tangential speed, and the second invariant of the strain-rate tensor on the penetrator nose surface are plotted in Fig. 7. With the recovery term in equation (15.5)

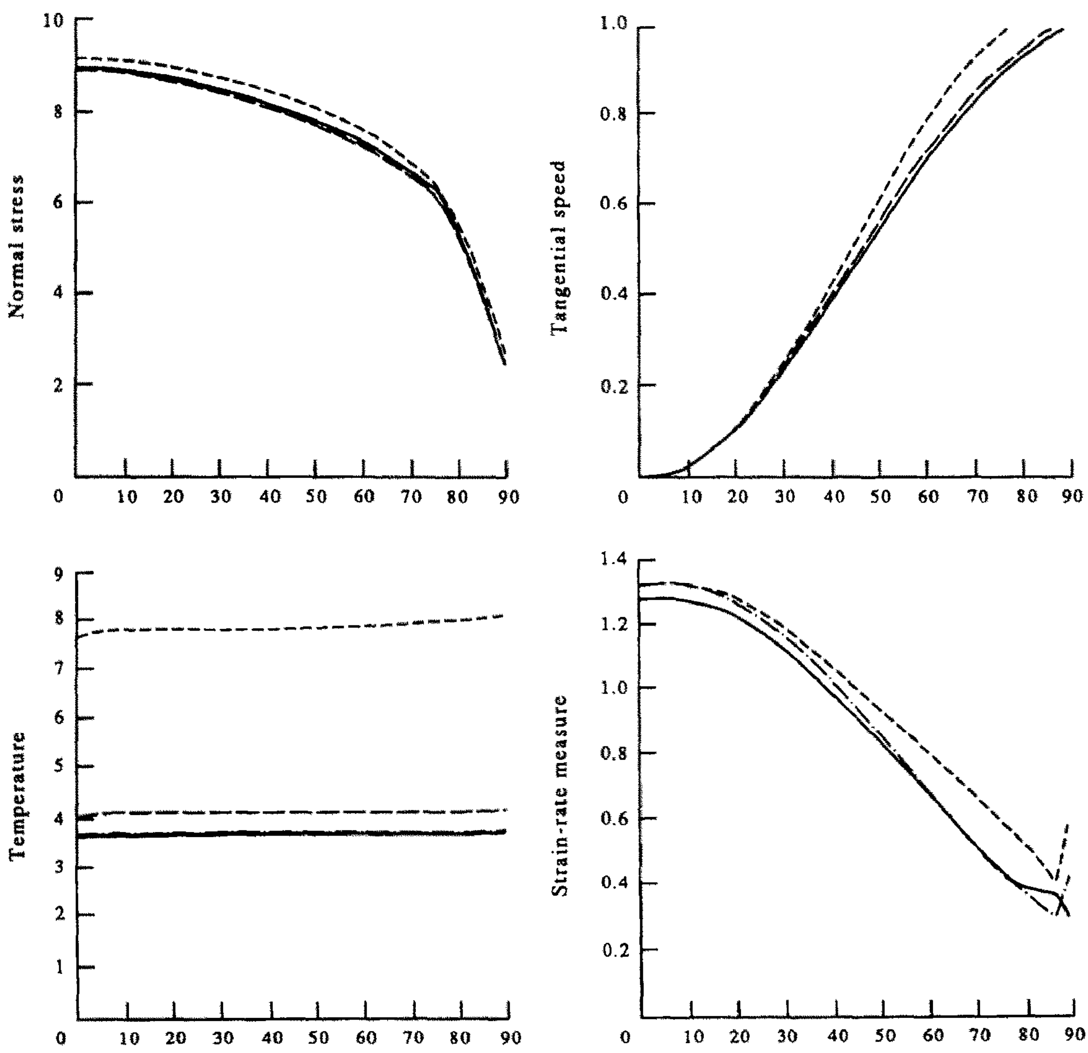

Fig. 7. Distribution of the normal stress, tangential speed, temperature rise, and the second invariant of the strain-rate tensor on the hemispherical nose surface of the penetrator for $\xi_2 = 100$ and four different values of ξ_1. —— no kinematic hardening; – – – $\xi_1 = 100$; ----- $\xi_1 = 10$; – · – $\xi_1 = 1.0$; – · · · – $\xi_1 = 0.1$.

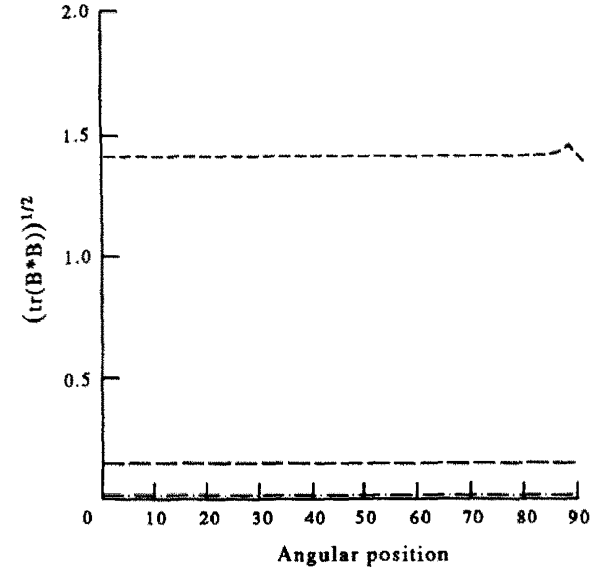

Fig. 8. Distribution of $(\mathrm{tr}(\mathbf{B}\,\mathbf{B}^{\mathrm{T}}))^{1/2}$ upon the penetrator nose surface for $\xi_2 = 100$ and four different values of ξ_1. See Fig. 7 for the legend to curves. The curve for $\xi_1 = 0.1$ coincides with the horizontal axis.

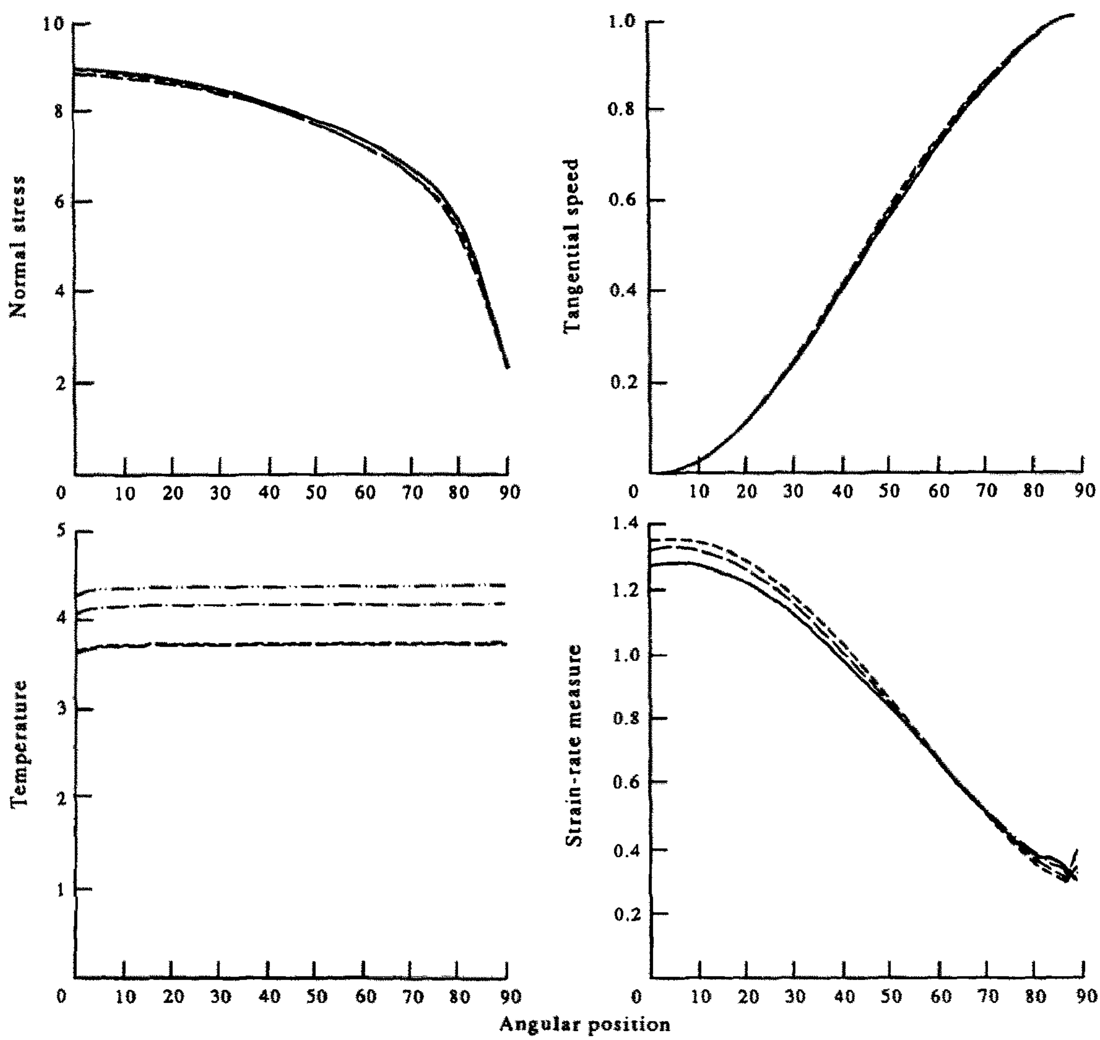

Fig. 9. Distribution of the normal stress, tangential speed, temperature rise, and the second invariant of the strain-rate tensor on the hemispherical nose surface of the penetrator for $\xi_2 = 10^6$ and four different values of ξ_1. —— no kinematic hardening; – – – $\xi_1 = 10^2$; ----- $\xi_1 = 10^4$; – · – $\xi_1 = 10^5$; – · · – $\xi_1 = 1.5 \times 10^5$.

fixed, an increase in the value of ξ_1 should result in higher values of **B**, as confirmed by the results included in Fig. 8, which in turn gives rise to higher values of the temperature. The computed results exhibit this behavior. The temperature distribution on the penetrator nose surface stays essentially uniform because of the convective transfer of heat. The values of the target resistance parameter $R_t = 8.84$, 8.01, 7.97, and 7.96 for $\xi_1 = 0.1$, 1, 10, and 100, respectively. The axial resisting force F experienced by the penetrator was found to be 7.76, 7.77, 7.82, and 8.10, respectively, for $\xi_1 = 0.1$, 1, 10, and 100. However, when ξ_2 was fixed at 10^6 and ξ_1 assigned values 10^2, 10^4, 10^5, and 1.5×10^5, the axial resisting force and the target resistance parameter were found to be 7.76 and 7.90, respectively, for all four values of ξ_1 considered. That higher values of ξ_1 result in more temperature rise at target particles abutting the penetrator nose surface is evidenced by results plotted in Fig. 9. However, the distribution of the normal stress and the tangential speed at points on the penetrator nose surface are affected very little, even when ξ_1 is increased by three orders of magnitude. Also, the hydrostatic pressure p at the stagnation point is not affected much by the consideration of kinematic hardening. For example, for $\xi_2 = 10^6$, p at the stagnation point equaled 8.34, 8.36, 8.22, and 8.18, respectively, for $\xi_1 = 10^2$, 10^4, 10^5, and 1.5×10^5. The contours of the hydrostatic pressure were virtually unchanged when the effect of kinematic hardening was considered.

Figure 10 depicts contours of $I_B \equiv (\mathrm{tr}(\mathbf{BB}^T))^{1/2}$ for $\xi_1 = \xi_2 = 1$. The contours of I_B are virtually parallel to the crater surface. On any radial line I_B drops off quite rapidly for a distance of r_0

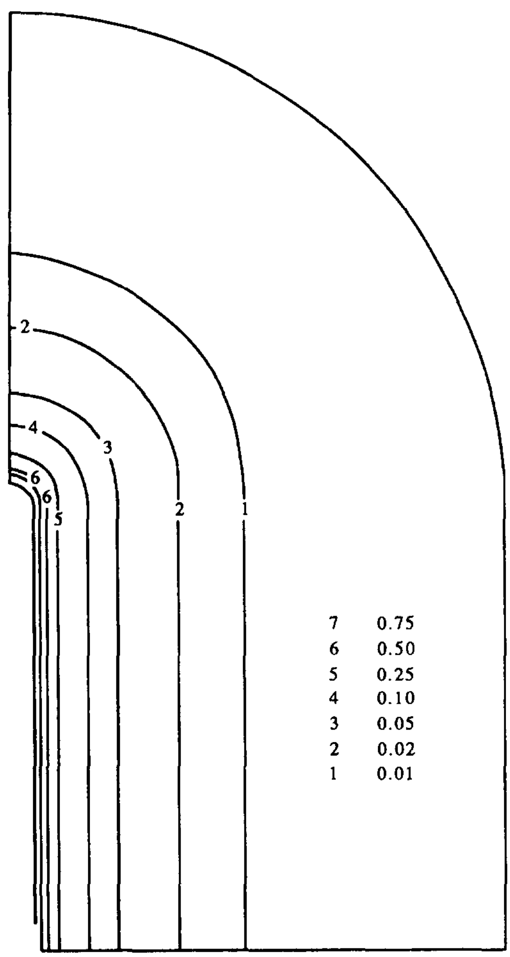

Fig. 10. Contours of $(\mathrm{tr}(\mathbf{B}\,\mathbf{B}^T))^{1/2}$ within the deforming target region.

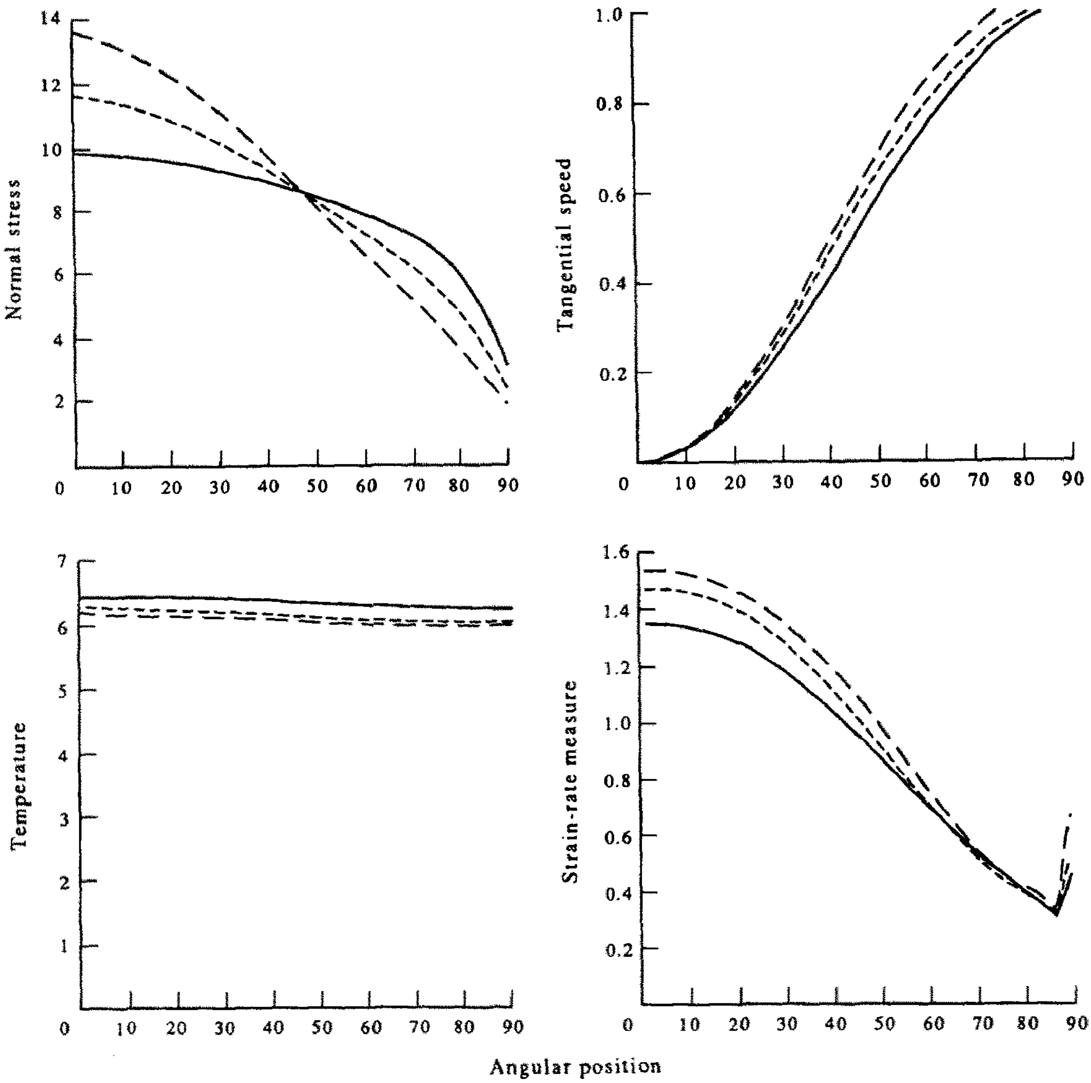

Fig. 11. Distribution of the normal stress, tangential speed, temperature rise, and the second invariant of the strain-rate tensor on the hemispherical nose surface of the penetrator for $\xi_1 = 1$, $\xi_2 = 100$, and three different values of α; —— $\alpha = 2$; ----- $\alpha = 6$; and – – – $\alpha = 10$.

from the crater surface, and then quite slowly. The contours of I_B for other values of ξ_1 and ξ_2 are similar to those shown in Fig. 10 and are not included herein.

3.3 *Results with α varied*

We have plotted in Fig. 11 the distribution on the penetrator nose surface of the normal stress, temperature rise, tangential speed, and the strain-rate measure for $\alpha = 2$, 6, and 10 with $\xi_1 = 1$ and $\xi_2 = 100$ kept fixed. The normal stress distribution on the penetrator nose surface resembles that computed by Batra and Wright [9] for the case of no kinematic hardening in the sense that its value at the point for which $\psi \approx 46°$ is unaffected by the value of α, and it increases with α for $\psi < 46°$ and decreases with α for $\psi > 46°$. We note that Batra and Wright used a coarse finite element mesh consisting of 6-noded triangular elements and considered a smaller target region than that studied herein. The values of the strain-rate measure increase with α for $\psi < 60°$, those of the tangential speed increase with α for $10° \le \alpha \le 80°$, and the temperature distribution on the penetrator nose surface is affected very little when α is increased from two to ten. The distribution of $(\mathrm{tr}(\mathbf{B}\,\mathbf{B}^T))^{1/2}$ on the penetrator nose surface,

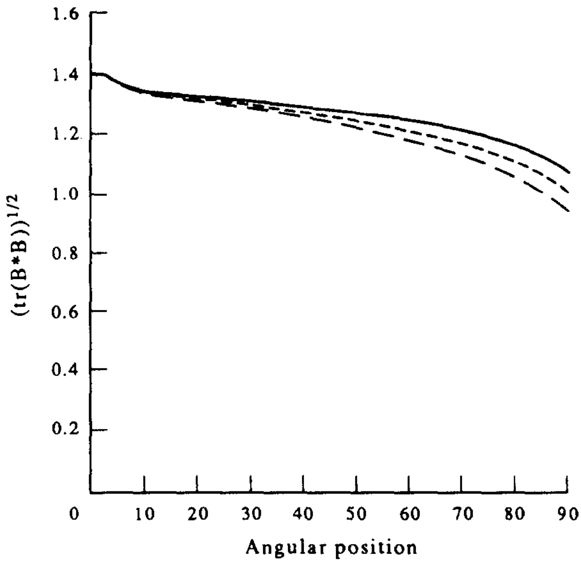

Fig. 12. Distribution of $(\mathrm{tr}(\mathbf{B}\,\mathbf{B}^T))^{1/2}$ upon the penetrator nose surface for $\xi_1 = 1$, $\xi_2 = 1$, and for $\alpha = 2$, 6, and 10. See Fig. 11 for the legend to the curves.

depicted in Fig. 12, shows that, at points near the nose periphery, I_B decreases with an increase in the value of α. The axial resisting force F experienced by the penetrator equals 8.57, 8.72, and 8.87 for $\alpha = 2$, 6, and 10, respectively. Results computed with $\xi_1 = 1$, and $\xi_2 = 100$ showed similar trends with a change in α, except that I_B was found to be uniformly distributed on the penetrator nose surface and equaled 0.014 for $\alpha = 2$, 6, and 10.

4. CONCLUSIONS

We have analyzed steady state axisymmetric thermomechanical deformations of a kinematically hardening viscoplastic target being penetrated by a fast moving hemispherical nosed rigid cylindrical rod. The deformations of the target appear to be steady to an observer situated at the penetrator nose tip. It is found that the consideration of kinematic hardening increases the normal stress and the temperature rise at a point on the penetrator nose surface. This increase in the normal stress is due to the evolution of the back stress and the values of the hydrostatic pressure at a point are changed very little when effects of kinematic hardening are included in the analysis. The kinematic hardening increases the values of the target resistance parameter appearing in Tate's modified Bernoulli equation.

Acknowledgements—This work was supported by the U.S. Army Research Office Contract DAAL03-92-G-0315 to the University of Missouri–Rolla. Some of the computations were performed on the NSF sponsored supercomputer center at the University of Illinois at Urbana–Champaign.

REFERENCES

[1] B. D. COLEMAN and M. E. GURTIN, *J. chem. Phys.* **47,** 597 (1967).
[2] K. S. CHAN, U. S. LINDHOLM, S. R. BODNER and K. P. WALKER, *Proceedings of 2nd Symposium on Nonlinear Constitutive Relations for High Temperature Applications* NASA Lewis Research Center (1984).
[3] T. INOUE, In *Thermal Stresses III* (Edited by R. B. HETNARSKI), pp. 192–278. North Holland, Amsterdam, (1989).
[4] J. LUBLINER, *Plasticity Theory.* Macmillan, New York (1990).
[5] L. ANAND, *Int. J. Plasticity* **1,** 213 (1985).
[6] R. C. BATRA and R. JAYACHANDRAN, *Int. J. Impact Engng* **12,** 209 (1992).

[7] S. R. BODNER and Y. PARTOM, *J. appl. Mech.* **42,** 385 (1975).
[8] S. B. BROWN, K. H. KIM and L. ANAND, *Int. J. Plasticity,* **5,** 95 (1989).
[9] R. C. BATRA and T. W. WRIGHT, *Int. J. Engng Sci.* **24,** 41 (1986).
[10] R. JAYACHANDRAN and R. C. BATRA, *Acta mech.* **92,** 9 (1992).
[11] R. C. BATRA and T. GOBINATH, *Int. J. Impact Engng.* **11,** 1 (1991).
[12] T. GOBINATH and R. C. BATRA, *Int. J. Engng Sci.* **29,** 1315 (1991).
[13] R. C. BATRA, *Int. J. Engng Sci.* **25,** 1131 (1987).
[14] R. C. BATRA, *Comp. Mech.* **3,** 1 (1988).
[15] R. C. BATRA and P.-R. LIN, *Int. J. Engng Sci.* **26,** 183 (1988).
[16] R. C. BATRA and P. R. LIN, *Int. J. Impact Engng.* **8,** 99 (1989).
[17] R. C. BATRA and P. R. LIN, *Int. J. Engng Sci.* **28,** 93 (1990).
[18] P. R. LIN and R. C. BATRA, *Int. J. Engng. Sci.* **27,** 1155 (1989).
[19] R. JAYACHANDRAN and R. C. BATRA, *Int. J. Engng Sci.* **30,** 1009 (1992).
[20] M. E. BACKMAN and W. GOLDSMITH, *Int. J. Engng Sci.* **16,** 1 (1978).
[21] T. W. WRIGHT and K. FRANK, *SMIRT Symposium,* No. 14. Impact, Lausanne, Switzerland (1987).
[22] C. E. ANDERSON and S. R. BODNER, *Int. J. Impact Engng* **7,** 9 (1988).
[23] T. Z. BLAZYNSKI, *Materials at High Strain Rates* (Edited by T. Z. BLAZYNSKI). Elsevier Applied Science, London (1987).
[24] M. MACAULEY, *Introduction to Impact Engineering.* Chapman & Hall, London (1987).
[25] J. A. ZUKAS *et al., Impact Dynamics.* Wiley–Interscience, New York (1982).
[26] J. A. ZUKAS (Ed.), *High Velocity Impact Dynamics.* Wiley–Interscience, New York (1990).
[27] G. BIRKHOFF, D. P. McDOUGALL, E. M. PUGH and G. TAYLOR, *Proc. Phys. Soc. Lond.* **57,** 147 (1945).
[28] D. C. PACK and W. M. EVANS, *Proc. Phys. Soc. Lond.* **B64,** 298 (1951).
[29] W. A. ALLEN and J. W. ROGERS, *J. Franklin Inst.* **272,** 275 (1961).
[30] V. P. ALEKSEEVSKII, *Comb. Expl. Shock Waves* **2,** 63 (1966). (Translation from Russian, Faraday Press, New York.)
[31] A. TATE, *J. Mech. Phys. Solids* **15,** 387 (1967).
[32] A. TATE, *J. Mech. Phys. Solids* **17,** 141 (1969).
[33] A. TATE, *Int. J. mech. Sci.* **28,** 535 (1986).
[34] A. TATE, *Int. J. mech. Sci.* **28,** 599 (1986).
[35] P. H. PIDSLEY, *J. Mech. Phys. Solids* **32,** 315 (1984).
[36] J. AWERBUCH, Technion–Israel Institute of Technology, MED Report No. 28 (1970).
[37] J. AWERBUCH and S. R. BODNER, *Int. J. Solids Struct.* **10,** 671 (1974).
[38] M. RAVID and S. R. BODNER, *Int. J. Engng Sci.* **21,** 577 (1983).
[39] M. RAVID, S. R. BODNER and I. HOLCMAN, *Int. J. Engng. Sci.* **25,** 473 (1987).
[40] M. J. FORRESTAL, K. OKAJIMA and V. K. LUK, *J. appl. Mech.* **55,** 755 (1988).
[41] R. C. BATRA and XINGJU CHEN, *Int. J. Engng. Sci.* **28,** 1347 (1990).
[42] X. CHEN and R. C. BATRA, *Acta mech.* **97,** 153 (1993).
[43] C. S. WHITE, C. A. BRÓNKHORST and L. ANAND, *Mech. Mater.* **10,** 127 (1990).
[44] Y. SHIMAZAKI and E. G. THOMPSON, *Int. J. numer Meth. Engng* **17,** 97 (1981).
[45] Y. M. WANG and R. C. BATRA, *Acta mech.* In press.

(Received 8 July 1992; accepted 25 August 1992)